Chemical Engineering Journal 401 (2020) 126135

Contents lists available at ScienceDirect

Chemical Engineering Journal

journal homepage: www.elsevier.com/locate/cej

Synchronous construction of CoS_2 in-situ loading and S doping for g-C_3N_4: Enhanced photocatalytic H_2-evolution activity and mechanism insight

Yazhou Zhang[a,b], Jinwen Shi[a,*], Zhenxiong Huang[a], Xiangjiu Guan[a], Shichao Zong[a], Cheng Cheng[a], Botong Zheng[a], Liejin Guo[a]

[a] International Research Center for Renewable Energy (IRCRE), State Key Laboratory of Multiphase Flow in Power Engineering (MFPE), Xi'an Jiaotong University (XJTU), 28 West Xianning Road, Xi'an 710049, China

[b] State Key Laboratory for Physical Chemistry of Solid Surfaces, Collaborative Innovation Center of Chemistry for Energy Materials, National & Local Joint Engineering Research Center for Preparation Technology of Nanomaterials, College of Chemistry and Chemical Engineering, Xiamen University, 422 Siming South Road, Xiamen 361005, China

HIGHLIGHTS

- CoS_2 in-situ loading and S doping for g-C_3N_4 are synchronously constructed.
- Partial N atoms in g-C_3N_4 are replaced by S atoms.
- CoS_2 nanosheets as H_2-evolution co-catalysts in-situ grow on the surface of g-C_3N_4 nanosheets.
- Co-S bonding between CoS_2 and S-doped g-C_3N_4 enhances directed transfer of photo-generated electrons.
- The noble-metal-free photocatalytic H_2-evolution activity of g-C_3N_4 is effectively elevated.

GRAPHICAL ABSTRACT

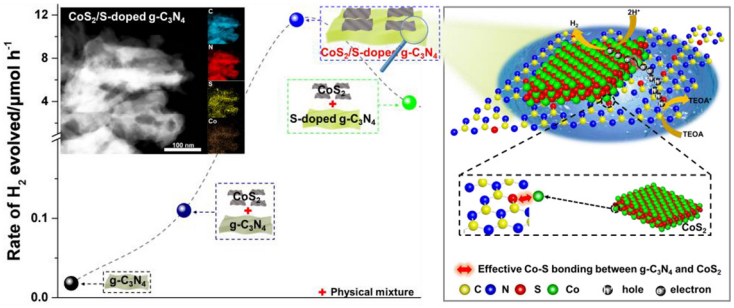

ARTICLE INFO

Keywords:
Photocatalysis
Hydrogen
Graphitic carbon nitride
Cobalt disulfide
Noble-metal-free
Co-S bonding

ABSTRACT

Considering the fact of the cost control in photocatalysis, it is significant to develop the noble-metal-free photocatalysis for H_2 evolution. Herein, CoS_2 in-situ loading and S doping for g-C_3N_4 were synchronously constructed by hydrothermal and sulfidation processes. With systematical physicochemical characterizations, it was found that partial N atoms in g-C_3N_4 were replaced by S atoms, improving the visible-light absorption ability for more generation of photo-generated carriers. CoS_2 as an effective noble-metal-free H_2-evolution cocatalyst induced and captured photo-generated electrons for promoting separation of photo-generated carriers synergistically with S doping. More contact between CoS_2 and g-C_3N_4 were formed by the in-situ growth of CoS_2 nanosheets on the surface of g-C_3N_4 nanosheets. It was important that Co-S bonding between CoS_2 and S-doped g-C_3N_4 was built by the synchronous construction of CoS_2 in-situ loading and S doping, strengthening the directed transfer of photo-generated electrons from S-doped g-C_3N_4 to CoS_2. Accordingly, the synergetic function of CoS_2 in-situ loading and S doping effectively elevated the noble-metal-free photocatalytic activity of g-C_3N_4 for H_2 evolution under visible-light irradiation.

* Corresponding author.
E-mail address: jinwen_shi@mail.xjtu.edu.cn (J. Shi).

https://doi.org/10.1016/j.cej.2020.126135
Received 8 April 2020; Received in revised form 15 June 2020; Accepted 28 June 2020
Available online 01 July 2020

1. Introduction

Photocatalytic water splitting for H_2 evolution is thought as one feasible way to realize the effective utilization of abundant solar energy in solving the energy crisis [1,2]. Since Fujishima and Honda found the photoelectrochemical phenomenon of TiO_2 photoelectrode for H_2 and O_2 evolution [3], comprehensive studies on photocatalysis have been deeply extended. Based on previous research works, suitable photocatalysts should be a key factor in the photocatalytic process [4,5]. Until now, representative photocatalysts, such as TiO_2 [6,7], $SrTiO_3$ [8,9], CdS [10,11], g-C_3N_4 [12–15], and GaN:ZnO [16–18], have been widely developed and applied in photocatalysis. Among these reported photocatalysts, g-C_3N_4 with graphite-like two-dimension (2D) microstructure has a lot of advantages, such as low cost, easy preparation, and suitable band gap [19–21]. However, the high recombination rate of photo-generated carriers always leads to its low efficiency in photocatalysis [22].

Generally, the adverse process of g-C_3N_4 can be well inhibited by modification of noble-metal cocatalysts with large work functions such as Pt and Au, inducing the migration of photo-generated electrons from g-C_3N_4 to the surfaces of noble metals and prevent recombination of photo-generated carriers [23,24]. It is known that noble metals are rare and extremely expensive. In consideration of the cost of photocatalysis, it is necessary to develop noble-metal-free cocatalysts as the replacement of noble metals.

It was widely reported that transition metal (Co, Ni, Fe, Cu)-based compounds, such as corresponding oxides, phosphides, sulfide, and hydroxides, possess favorable electrochemical abilities for H_2-evolution reaction (HER) [25–27]. Moreover, several research groups proved that some (Co, Ni, Fe, Cu)-based compounds performed comparable HER activities to noble metals under some conditions [26]. It is suggested that most of materials with favorable electrochemical abilities always show the potential application in photocatalytic field, and (Co, Ni, Fe, Cu)-based compounds have been indeed applied as cocatalysts in photocatalysis [26]. As for g-C_3N_4, noble-metal-free (Co, Ni, Fe, Cu)-based compounds, such as Ni_xP [28,29], NiS [30], Co_xP [13,31,32], Fe_xP [33], Cu_3P [34], and Ni/NiO [35], were successfully applied as noble-metal-free cocatalysts to elevate its photocatalytic ability. Meanwhile, it is reported that the microstructures of cocatalysts have a significant influence on contact with photocatalysts as well as the generation of active sites, which is also important to improve photocatalytic ability [36–38]. Until now, the low noble-metal-free photocatalytic efficiency and the unclear interaction mechanism between g-C_3N_4 and noble-metal-free cocatalysts severely hindered photocatalytic application of g-C_3N_4, implying that more efforts should be provided to conquer these problems.

Cobalt sulfide has low Gibbs free energy for hydrogen adsorption [39], and is recognized as one of the potential cocatalysts for H_2 evolution. There are only rare reports about cobalt sulfide such as CoS nanoparticles or CoS_x polyhedrons, acting as H_2-evolution cocatalysts for the enhanced noble-metal-free photocatalytic performance of g-C_3N_4 [38,40]. It is deserved that more efforts should be taken to develop cobalt sulfide with special microstructures coupling with g-C_3N_4 for better noble-metal-free photocatalytic ability. Recently, it was reported that CoS_2-based 2D nanosheets were developed as one of the excellent electrocatalysts for HER [41]. Based on the above mentioned, CoS_2 nanosheets are expected to function as one favorable cocatalyst of g-C_3N_4 to improve photocatalytic ability.

Furthermore, the relatively wide bandgap (~2.7 eV) of g-C_3N_4 signified its weak visible-light absorption ability [19], and effective light absorption is responsible for the generation of photo-generated carriers, which is essential to promote utilization of more carriers in photocatalysis [2]. Cocatalysts are commonly unable to improve the light absorption ability of g-C_3N_4. It is expected that a suitable strategy for better light absorption ability couples with CoS_2 nanosheets loading to enhance generation and separation of photo-generated carriers. Doping strategy, especially doping of nonmetal elements, is proved to be beneficial to improve light absorption of g-C_3N_4 and elevate the photocatalytic performance [42]. Considering these facts, it is thought that S doping is more feasible to combine with CoS_2 loading. Moreover, S-doped g-C_3N_4 was reported to realize good visible-light response and promote the generation and transfer of carriers [43–45].

In this work, g-C_3N_4 was prepared by the thermolysis of urea, and then CoS_2 in-situ loading and S doping on g-C_3N_4 were synchronously realized by hydrothermal and sulfidation processes. Based on comprehensive physicochemical characterizations analyzation, CoS_2 nanosheets as effective H_2-evolution cocatalysts were verified to tightly anchor to g-C_3N_4, while S atoms substituted for partial N atoms in g-C_3N_4. The coupling mechanism between CoS_2 and S-doped g-C_3N_4 was studied in detail. It was found that the synchronous construction of CoS_2 in-situ loading and S doping could promote effective combination between CoS_2 and S-doped g-C_3N_4 and then induce the formation of strong Co-S bonding between CoS_2 and S-doped g-C_3N_4, subsequently improving noble-metal-free photocatalytic H_2-evolution activity under visible-light irradiation.

2. Experimental section

2.1. Chemicals

Urea (CH_4N_2O), sodium dodecyl sulfate ($C_{12}H_{25}SO_4Na$), cobalt nitrate hexahydrate ($Co(NO_3)_2{\cdot}6H_2O$), hexamethylenetetramine ($C_6H_{12}N_4$), ethanol (C_2H_6O), sodium sulfate (Na_2SO_4), sulfur powder, and Triethanolamine ($C_6H_{15}NO_3$,TEOA) were purchased from Sinopharm Chemical Reagent Co., Ltd. Chloroplatinic acid hexahydrate ($H_2PtCl_6{\cdot}6H_2O$) was purchased from Alfa Aesar. Nafion® solutions (D1020, 10 wt%) was purchased from Dupont. All chemicals were analytical grade and used without further purification. Deionized water with a resistivity (18.2 MΩ·cm) was used in all experiments.

2.2. Preparation

g-C_3N_4 is prepared by thermal condensation of the precursor urea. Firstly, urea (10.0 g) was added into one crucible and covered with a lid. Then the crucible was moved into a furnace and heated up to 550 °C with a heating rate of 5 °C min^{-1} and kept for 4 h. Finally, after naturally cooling down to room temperature, g-C_3N_4 was obtained and labeled as CN.

CoS_2 is prepared according to the reported work [41]**.** Firstly, sodium dodecyl sulfate (5 mmol, 1441.90 mg), cobalt nitrate hexahydrate (1 mmol, 291.03 mg) and hexamethylenetetramine (6 mmol, 841.12 mg) were orderly dissolved into deionized water (22 mL) with stirring. The solution was then moved into a Teflon-lined autoclave and kept at 120 °C for 24 h. After naturally cooling down to room temperature, the precipitation was washed three times by deionized water and one time by ethanol, and dried in vacuum for 12 h at 60 °C. The obtained powders were thoroughly mixed with sulfur powder (50 mg), and then heated to 350 °C with a heating rate of 5 °C min^{-1} and kept for 2 h in Ar atmosphere. Finally, after naturally cooling down to room temperature, the obtained black powders were collected and labeled as CoS_2.

CoS_2/S-doped g-C_3N_4 is prepared by hydrothermal and sulfidation processes similar to those of CoS_2 except that CN was added in the hydrothermal solution. Firstly, CN (200 mg) was dispersed into deionized water (22 mL) by sonication for 30 min. Then sodium dodecyl sulfate (0.24 mmol, 69.21 mg), cobalt nitrate hexahydrate (0.048 mmol, 13.97 mg) and hexamethylenetetramine (0.288 mmol, 40.37 mg) were orderly dissolved into the above suspension with stirring. The formed suspension was moved into a Teflon-lined autoclave and then kept at 120 °C for 24 h. After naturally cooling down to room temperature, the precipitate was washed three times by deionized water and one time by ethanol, and dried in vacuum for 12 h at 60 °C.

The obtained powders were enough mixed with sulfur powder (50 mg), and then heated to 350 °C with a heating rate of 5 °C min^{-1} and kept for 2 h in Ar atmosphere. Finally, after naturally cooling down to room temperature, g-C_3N_4 loaded with 3 wt% CoS_2 was obtained and labeled as CN-3CoS_2. Samples with other weight contents of CoS_2 (2, 6 wt%) were prepared based on the same process by controlling the added weight of cobalt nitrate hexahydrate and keeping the constant molar ratios between sodium dodecyl sulfate, cobalt nitrate hexahydrate and hexamethylenetetramine. The obtained samples were labeled as CN-*x*CoS_2, in which × wt% represents the weight ratio of CoS_2 and g-C_3N_4.

S-doped g-C_3N_4 named as CN-HTS was prepared by the same process of CN-3CoS_2 without the existence of cobalt nitrate hexahydrate, and the S-doped g-C_3N_4 named as CN-WHTS was prepared by the same process of CN-HTS without the existence of sodium dodecyl sulfate and hexamethylenetetramine.

Physical mixture samples were prepared as follows: CN, CN-HTS or CN-WHTS (100 mg) and CoS_2 (3 mg) were added into ethanol (10 mL), kept in sonication for 30 min and then stirred for 2 h. Then the suspension was dried in vacuum for 12 h at 60 °C, and the obtained powders were labeled as CN + 3CoS_2, CN-HTS + 3CoS_2 or CN-WHTS + 3CoS_2, respectively.

2.3. Physicochemical characterization

For X-ray diffraction (XRD) patterns, a diffractometer (PANalytical X'pert Pro MPD, Netherlands) was used with a scan rate of 2° min^{-1} in the 2θ range from 10 to 80° under Ni-filtered Cu Kα irradiation. For Scanning electron microscopy (SEM), a field-emission scanning electron microscope (JEOL JSM-7800F, Japan) was used under an accelerating voltage (3 kV). For Transmission electron microscopy (TEM), a transmission electron microscope (JEOL JEM-F200, Japan) for CN-3CoS_2 sample was employed under an accelerating voltage (200 kV), and a transmission electron microscope (FEI Tecnai G^2 F30 S-Twin, USA) for CoS_2 sample was employed under an accelerating voltage (300 kV). For Brunauer-Emmette-Teller (BET) surface area measurement, an accelerated surface area and porosimetry analyzer (Micromeritics ASAP 2020, USA) was used with N_2-adsorption/desorption isotherms. For Fourier transform infrared (FTIR) spectra, an FTIR spectrophotometer (Bruker Vertex70, Germany) was applied with the wavenumber range (4000–400 cm^{-1}). For X-ray photoelectron spectroscopy (XPS), an X-ray photoelectron spectroscope (Kratos Axis Ultra DLD, Japan) was used with a monochromatic Al Kα line source (hν = 1486.69 eV), and the reference was the adventitious C 1s peak at 284.8 eV. For UV–Vis spectra, a UV–Vis-near-IR spectrophotometer (Agilent Cary 5000, USA) was applied with $BaSO_4$ reference in the range (350–800 nm). For Photoluminescence spectra (PL), a steady-state fluorescence spectrophotometer (PTI QuantaMaster 40, USA) was used equipped with an excitation wavelength of 377 nm under room temperature.

2.4. Electrochemical measurement

Electrodes were prepared by a simple dropping method. The mixture including corresponding photocatalyst powders (1 mg), deionized water (250 μL), ethanol (250 μL) and Nafion® solutions (10 μL) was sonicated for 30 min. The obtained dispersion (2.5 μL) was dropped on the glassy carbon electrode (3 mm diameter), and then dried at room temperature overnight. The synthesized electrodes based on CN, CN-HTS and CN-3CoS_2 were labeled as CN-E, CN-HTS-E and CN-CoS_2-E, respectively.

Electrochemical measurement was carried out by a bipotentiostat (CH Instruments, China). The carbon rod, Ag/AgCl electrode and as-prepared electrode were used as the counter electrode, reference electrode and working electrode, respectively. Meanwhile, Na_2SO_4 (0.5 M, pH = 6.8) aqueous solution was applied as electrolyte. Linear sweep voltammetry (LSV) curves were recorded at a scan rate of 0.01 V s^{-1}, and the current densities were normalized to the geometrical surface area. The potential vs Ag/AgCl were converted to corresponding potential vs Reversible Hydrogen Electrode (RHE) based on the following equation:

$$E_{RHE} = E_{Ag/AgCl} + 0.059 \times pH + E^0_{Ag/AgCl} \quad (E^0_{Ag/AgCl} = 0.1976\ V \text{ at } 25\ ^\circ C) \tag{1}$$

2.5. Photoelectrochemical measurement

Photoelectrodes were prepared by a simple dropping method. The suspension was prepared and composed of as-prepared photocatalyst (5 mg), ethanol (1 mL) and Nafion solutions (20 μL), and then kept ultrasonic for 30 min. Then the suspension (200 μL) was dropped onto as-cleaned FTO glass (1.0 × 1.5 cm^2), and dried at 70 °C for 2 h in air. The obtained photoelectrodes based on CN and CN-3CoS_2 were labeled as CN-PA and CN-CoS_2-PA, respectively.

A three-electrode cell was composed of the counter electrode (Pt slice), the reference electrode (Ag/AgCl) and the working electrode (the prepared photoelectrodes), was applied for photoelectrochemical measurement, and Na_2SO_4 aqueous solution (0.5 M, pH = 6.8) was chosen as the electrolyte. The transient photocurrent densities were obtained at an applied voltage (0.5 V vs Ag/AgCl). Electrochemical impedance spectroscopy (EIS) were recorded with the frequency range (100 kHz − 1 Hz) and an applied voltage (0.5 V vs Ag/AgCl) under visible-light irradiation. The transformation of potentials vs Ag/AgCl and RHE was calculated by the Eq. (1).

2.6. Photocatalytic measurement

Photocatalytic H_2-evolution activities were measured in a Pyrex glass cell (100 mL) with side irradiation. A Xe lamp (300 W) equipped with a UV-cutoff filter ($\lambda > 420$ nm) was used as the visible-light source. In the photocatalytic system, TEOA functioned as the sacrificial agent to consume photo-generated holes. In detail, photocatalysts (20 mg), TEOA (8 mL) and deionized water (72 mL) were mixed into the glass cell with stirring. If CN was loaded with Pt cocatalyst by the in-situ photo-deposition method, the additional Pt resource (as-prepared H_2PtCl_6 aqueous solution) was also added into the mixed suspension. Then the cell was purged with Ar for 15 min to eliminate air, and sealed by clean latex plug. The generated H_2 in the photocatalytic process was evaluated by a gas chromatogram with a TDX-01 column and the carrier gas of high-purity Ar.

The measurement of apparent quantum yield (AQY) was carried out under the above Xe lamp equipped with different band-pass filters (420, 450, and 520 nm). The intensity of irradiated light was recorded from a spectroradiometer (Avantes AvaSpec-2048-USB2, Netherlands). The AQY value was obtained by the following Eq. (2):

$$\begin{aligned} AQY(\%) &= \frac{\text{Number of reacted electrons}}{\text{Number of incident photons}} \times 100 \\ &= \frac{\text{Number of evolved } H_2 \text{ molecules} \times 2}{\text{Number of incident photons}} \times 100 \end{aligned} \tag{2}$$

3. Results and discussion

XRD patterns of CN, CN-HTS and CN-3CoS_2 are shown in Fig. 1a. For CN, the characteristic peaks at around 12.9° and 27.3° were related to (1 0 0) and (0 0 2) diffraction facets of g-C_3N_4, respectively [46]. The former was caused by the in-plane repeating units of the continuous heptazine in g-C_3N_4, while the latter was attributed to the interlayer stacking of carbon nitride nanosheets [47]. There was no obvious difference among XRD patterns of CN, CN-HTS and CN-3CoS_2. It was verified from Fig. 1b that the prepared cobalt sulfide sample belonged to CoS_2 and showed weak crystallinity, meaning that the cobalt sulfide loading on g-C_3N_4 was the CoS_2 species of cobalt sulfide [41,48].

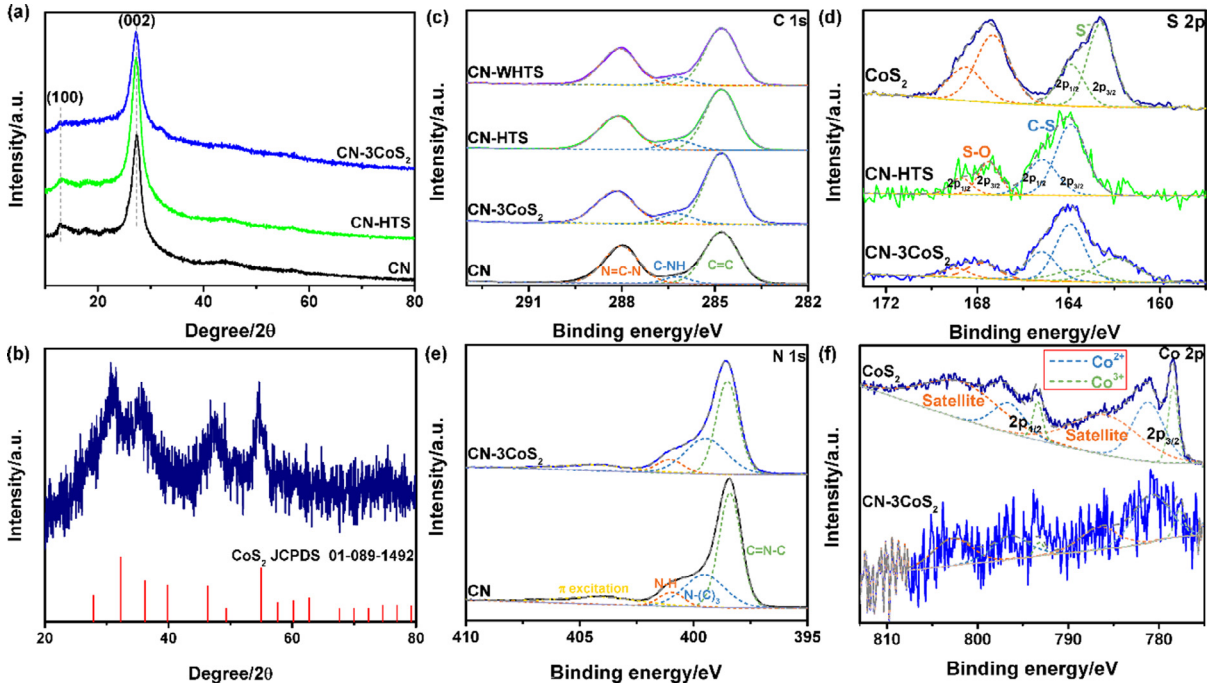

Fig. 1. (a) XRD patterns for CN, CN-HTS and CN-3CoS_2; (b) XRD pattern for CoS_2; (c) XPS C 1s spectra for CN, CN-3CoS_2, CN-HTS and CN-WHTS; (d) XPS S 2p spectra for CN-3CoS_2, CN-HTS and CoS_2; (e) XPS N 1s spectra for CN and CN-3CoS_2; (f) XPS Co 2p spectra for CN-3CoS_2 and CoS_2.

However, characteristic peaks of CoS_2 were not seen in the XRD pattern of CN-3CoS_2, which was attributed to the low CoS_2 loading content and the weak crystallinity of CoS_2. As observed from FTIR spectra (Fig. S1b), both CN and CN-3CoS_2 had the characteristic peaks at 3100–3500, 1200–1600 and 813 cm^{-1}, corresponding to the stretching vibration of N–H and O–H, characteristic stretching vibration mode and breathing mode of aromatic heptazine rings, respectively [49]. It was noted that any obvious difference could not be observed between the FTIR spectra of CN and CN-3CoS_2. Therefore, based on XRD and FTIR results, CoS_2 in-situ loading as well as the hydrothermal and sulfidation treatment had no obvious influence on the structure of g-C_3N_4.

However, the influence of CoS_2 in-situ loading as well as the hydrothermal and sulfidation treatment should be present from our experience, and then XPS characterization for precise structure analysis was carried out. Fig. 1c exhibits C 1s spectra for CN, CN-3CoS_2, CN-HTS and CN-WHTS. For CN, three characteristic peaks at 284.8, 286.2 and 288.0 eV were related to C=C, C–NH and sp^2-hybridized carbon in aromatic ring (N=C–N), respectively [12,50]. The corresponding characteristic peaks for CN-3CoS_2 were positioned at 284.8, 286.2 and 288.2 eV, respectively. It was notable that the peak (N=C–N) for CN-3CoS_2 had higher binding energy than that for CN, which implied that the chemical environment around C in N=C–N had some change by CoS_2 in-situ loading process. Meanwhile, the peak related to Co-C bond was not observed [51]. XPS C 1s spectra for CN-HTS and CN-WHTS were also measured to check whether the peak shift was caused by the hydrothermal and sulfidation treatment in the CoS_2 in-situ loading process. The relevant C 1s peaks for CN-HTS were at 284.8, 286.2 and 288.2 eV, while the relevant C 1s peaks of CN-WHTS were at 284.8, 286.2 and 288.1 eV. The C 1s peaks (N=C–N) of CN-HTS and CN-WHTS both showed higher binding energies than that of CN. It meant that the hydrothermal and sulfidation treatment should be responsible for the peak shift above mentioned, and it was speculated that partial S atoms might be doped into g-C_3N_4 in the preparation process of CN-3CoS_2, CN-HTS and CN-WHTS. To further verify the inference, S 2p spectra for CN-HTS, CN-3CoS_2 and CoS_2 were analyzed and shown in Fig. 1d. For CoS_2, the peaks at 162.6 and 163.8 eV were attributed to $2p_{3/2}$ and $2p_{1/2}$ of S^- in the S-Co of CoS_2, respectively [48,52]. The peaks (167.3 and 168.5 eV) corresponding to S-O were caused by partial oxidization of the surface sulfur species in air according to the existence of SO_4^{2-} at the preparation process [52–54]. For CN-HTS, the characteristic peaks at 163.9 and 165.2 eV were related to $2p_{3/2}$ and $2p_{1/2}$ of C-S, respectively [45,55]. It indicated that partial S atoms should be doped into positions of N atoms in g-C_3N_4 by the sulfidation process in the absence of Co source in association with C 1s results [43]. The peaks due to partial oxidization of the surface sulfur species were also seen in CN-HTS. In S 2p spectra of CN-3CoS_2, the characteristic peaks (163.9 and 165.2 eV) due to C-S were also observed, implying that S doping was synchronously carried out in CoS_2 in-situ loading process. Meanwhile, the peaks corresponding to $2p_{3/2}$ and $2p_{1/2}$ of S^- were positioned at 161.9 and 163.5 eV, respectively, and showed obvious shift compared with those of CoS_2. It should be attributed to the chemical surrounding change of S^- in CoS_2 after the combination with S-doped g-C_3N_4.

To further verify the influence of S doping, N 1s spectra for CN and CN-3CoS_2 were analyzed and shown in Fig. 1e. The characteristics peaks at 398.4, 399.5, 401.0 and 404.0 eV for CN were assigned to sp^2-hybridized N in aromatic rings (C–N=C), N-$(C)_3$ groups, amino functions (N–H) and π excitation, respectively [56]. For CN-3CoS_2, the corresponding characteristic peaks were positioned at 398.5, 399.5, 401.0 and 404.3 eV. The peak of N in aromatic rings had a little shift to high binding energy, which was attributed to the substitution of the doped S atoms for partial N atoms in the structure of g-C_3N_4. No signal about N 1s of Co-N bond could be observed [57]. Meanwhile, the chemical valence states of Co element in CoS_2 and CN-3CoS_2 were checked and observed from Fig. 1f. The peaks at 781.2 and 796.6 eV for CoS_2 were due to $2p_{3/2}$ and $2p_{1/2}$ of Co^{2+}, respectively, while the peaks at 785.9 and 801.8 eV belonged to two shake-up satellites [38,58]. Meanwhile, the weak Co^{3+} signals (778.4 and 793.4 eV) were also found, which was commonly existed in CoS_2 materials [52]. Co 2p signals in CN-3CoS_2 were very weak due to the low loading content of CoS_2 corresponding to XRD and FTIR results. The characteristic peaks of Co^{2+} (780.9 and 796.4 eV) slightly shifted to low binding energies compared with those of CoS_2. Considering the chemical surrounding change of S^- from S 2p result as well as the absence of Co–C or Co–N

bonds from C 1s and N 1s results, Co of CoS_2 should form the chemical bonding (Co-S) with the doped S in g-C_3N_4, then causing the binding energy shift of Co^{2+} and S^- in CN-3CoS_2. In addition, from Fig. S2b, only O signals of surface hydroxy (–OH) and chemisorbed water (H-O–H) were observed for CN-3CoS_2 and CoS_2 [59], and the absence of the metal-bonded oxygen signal proved that cobalt oxide species were inexistent in CoS_2/S-doped g-C_3N_4. Therefore, it was summarized that CoS_2 in-situ loading and S doping of g-C_3N_4 were synchronously realized, and the Co-S bonding was established between CoS_2 and S-doped g-C_3N_4 in CoS_2/S-doped g-C_3N_4.

Then the influence of CoS_2 in-situ loading and S doping on the band structure of g-C_3N_4 was checked by XPS VB spectra. As observed from Fig. S2c, the deduced valence band maximum (VBM) values for CN, CN-3CoS_2 and CN-HTS were around 2.12, 2.05 and 2.05 eV (vs. the Fermi level (E_F)), respectively. It stated that the VBM of CN was 0.07 eV more positive than those of CN-3CoS_2 and CN-HTS. Meanwhile, the same VBM values of CN-3CoS_2 and CN-HTS implied that S doping was the key to elevate the VBM of g-C_3N_4.

Further, it was necessary to check the light absorption ability of g-C_3N_4 with the synchronous construction of CoS_2 in-situ loading and S doping based on the fact of the structure change of g-C_3N_4 from XPS result. It was obviously observed from Fig. 2a that the absorption edge of CN was positioned at around 464 nm, and the corresponding bandgap was 2.67 eV. As for CN-HTS, the absorption edge (471 nm) showed obvious red-shift compared with that of CN, and the improved visible-light absorption ability should be caused by S doping matched with XPS results [60,61]. The stronger background absorption (450–800 nm) of CN-HTS than CN might be due to introduced deficiency by S doping. CN-3CoS_2 showed a stronger visible-light absorption ability than CN, and the position of the absorption edge (471 nm) was the same as that of CN-HTS, which implied that the absorption edge red-shift of g-C_3N_4 was attributed to S doping not CoS_2 in-situ loading. The stronger background absorption (450–800 nm) of CN-3CoS_2 than CN-HTS should be related to the additional light absorption by the introduction of black CoS_2 with whole visible-light absorption (Fig. 2a) [38,40]. Based on XPS and UV–Vis results, the relative band structures of CN, CN-3CoS_2 and CN-HTS were provided (Fig. 2b). The conduction band minimum (CBM) of CN was 0.03 eV more positive than that of CN-3CoS_2 or CN-HTS, which was helpful to promote the photocatalytic water reduction rection of g-C_3N_4.

The combination between g-C_3N_4 and CoS_2 at the micro-nano scale was checked by SEM and TEM. As observed from Fig. S4a and S4b, CN was composed of aggregated nanosheets [62], and there was no obvious difference between the microstructures of CN and CN-3CoS_2. CoS_2 had a microstructure of aggregated 2D nanosheets with the uniform distribution of Co and S [41], and showed the amorphous property due to the weak crystallinity of CoS_2 matched with XRD results (Fig. S5). For CN-3CoS_2, no obvious lattice fringes could be observed from the HRTEM image (Fig. 2c and 2d). Hence it was difficult to distinguish g-C_3N_4 and CoS_2 in the microstructure of CN-3CoS_2 because of their similar 2D nanosheet microstructures and amorphous properties. To explore the microstructure combination between g-C_3N_4 and CoS_2, STEM mapping images of CN-3CoS_2 were measured and exhibited in Fig. 2e. C, N, S and Co elements were uniformly distributed in CN-3CoS_2, implying that CoS_2 nanosheets should in-situ grow on the surface of g-C_3N_4 nanosheets and then tightly anchor to g-C_3N_4 nanosheets based on the formation of Co-S bonding from XPS result. Meanwhile, from nitrogen adsorption/desorption isotherms in Fig. S6, the similar BET surface areas of CN (70.4 $m^2\ g^{-1}$) and CN-3CoS_2 (70.9 $m^2\ g^{-1}$) indicated that CoS_2 in-situ loading and S doping had no obvious influence

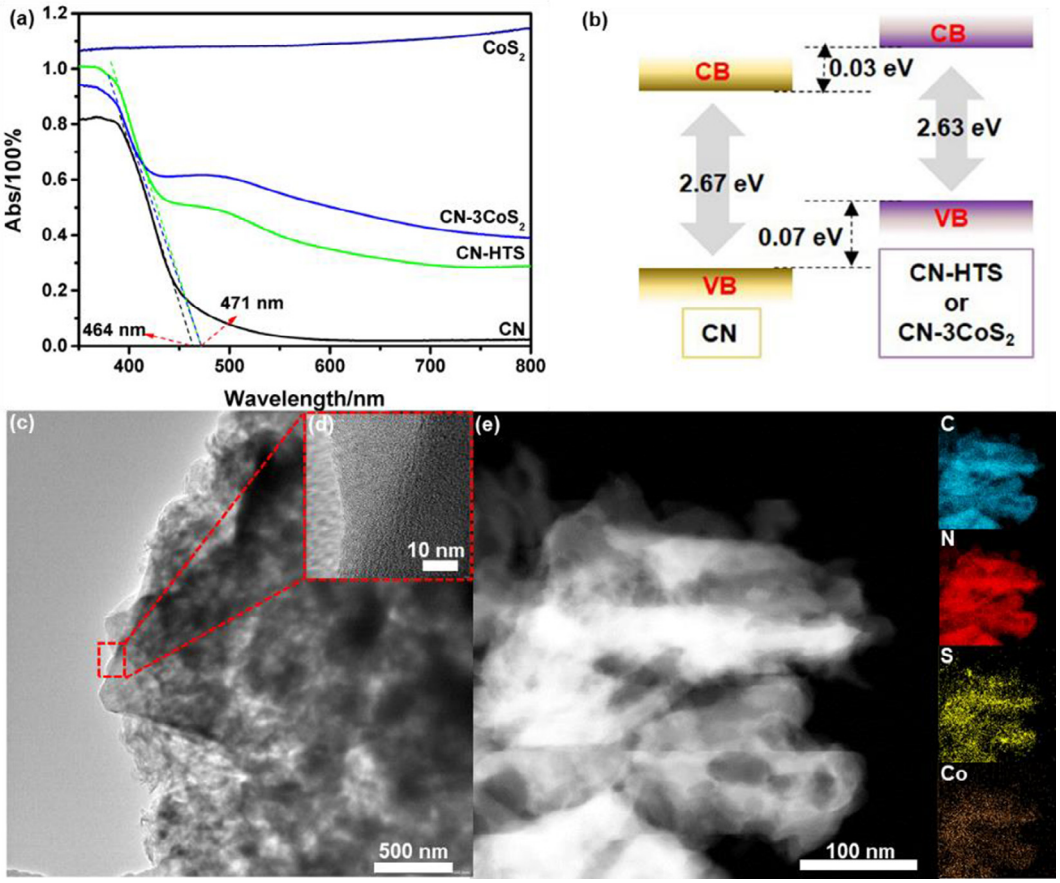

Fig. 2. (a) UV–Vis spectra for CN, CN-HTS, CN-3CoS_2 and CoS_2; (b) relative band structures for CN, CN-3CoS_2 and CN-HTS; (c) TEM image, (d) HRTEM image and (e) STEM mapping images for CN-3CoS_2.

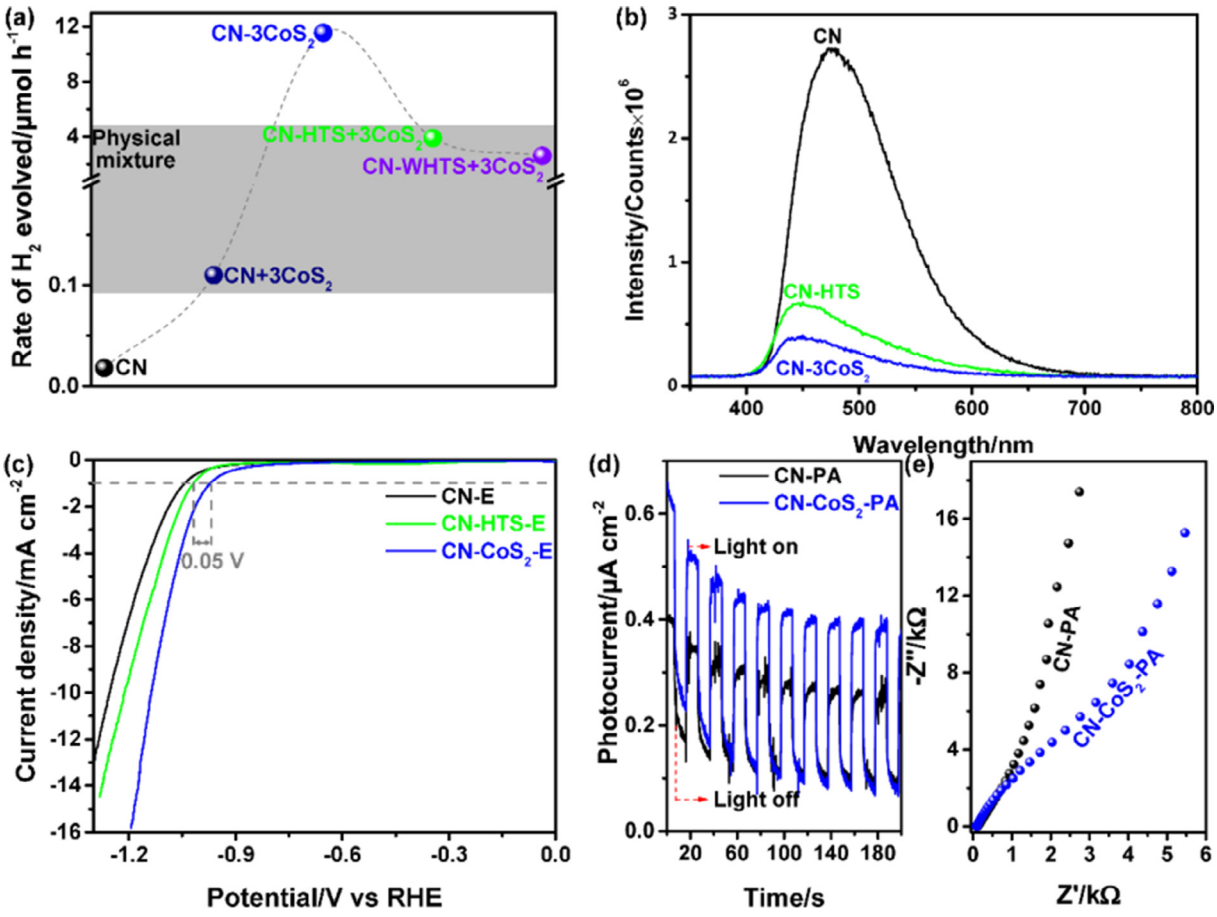

Fig. 3. (a) visible-driven photocatalytic H_2-evolved rates for CN, CN + $3CoS_2$, CN-$3CoS_2$, CN-HTS + $3CoS_2$ and CN-WHTS + $3CoS_2$; (b) PL spectra of CN, CN-$3CoS_2$ and CN-HTS; (c) HER performance for CN-E, CN-HTS-E and CN-CoS_2-E; (d) Transient photocurrent densities and (e) EIS spectra for CN-PA and CN-CoS_2-PA.

on the surface area of g-C_3N_4, further proving the in-situ growth of CoS_2 nanosheets on the surface of g-C_3N_4 nanosheets. Furthermore, the nanosheet microstructure of CoS_2 was beneficial to form more contact with g-C_3N_4.

Based on the above, it was obtained that Co-S bonding was formed between CoS_2 and S-doped g-C_3N_4, and CoS_2 nanosheets tightly anchored to g-C_3N_4 nanosheets by the synchronous construction of CoS_2 in-situ loading and S doping. Then the relationship between photocatalytic performance and synchronous construction of CoS_2 in-situ loading and S doping was investigated. As observed from Fig. 3a and S7a, CN only had quite weak photocatalytic activity (0.02 μmol h^{-1}) [31,38]. Photocatalytic activity of g-C_3N_4 was greatly enhanced by synchronous construction of CoS_2 in-situ loading and S doping, and CN-$3CoS_2$ had the best performance (11.55 μmol h^{-1}), which was around 578 times higher than that of CN (Fig. S7a). No H_2 gas could be detected in photocatalytic measurement process of CoS_2 sample. It proved that CoS_2 could act as an effective H_2-evolution cocatalyst and improve the photocatalytic activity of g-C_3N_4, corresponding to the cocatalyst function of cobalt sulfide in the photocatalytic study of g-C_3N_4 for H_2 evolution [38,40]. Meanwhile, CN-$3CoS_2$ showed favorable photocatalytic stability (Fig. S7b). To further verify the cocatalyst function of CoS_2 and check the interaction between S-doped g-C_3N_4 and CoS_2, some control samples (CN + $3CoS_2$, CN-HTS + $3CoS_2$ and CN-WHTS + $3CoS_2$) were prepared, and their photocatalytic activities are shown in Fig. 3a. Firstly, although all control samples were prepared by the method of physical mixture, they showed better photocatalytic performances compared with CN, which verified the effective cocatalyst function of CoS_2. CN + $3CoS_2$ exhibited photocatalytic activity (0.11 μmol h^{-1}), which was around 6 times that of CN. It was worth noting that CN + $3CoS_2$ had extremely weaker activity than CN-HTS + $3CoS_2$ (3.89 μmol h^{-1}) and CN-WHTS + $3CoS_2$ (2.61 μmol h^{-1}). It proved that S doping worked as the key factor to effectively promote the contact between g-C_3N_4 and CoS_2. Moreover, lower activities of all the control samples than that of CN-$3CoS_2$ implied that effective combination was formed between S-doped g-C_3N_4 and CoS_2 in synchronous construction processes of CoS_2 in-situ loading and S doping, and it was thought that effective combination was shown as Co-S bonding between CoS_2 and S-doped g-C_3N_4 based on XPS and TEM results. The AQYs at 420, 450 and 520 nm for CN-$3CoS_2$ were 1.08%, 0.6% and 0.02%, respectively. Based on the strong background absorption (450–800 nm) of CN-$3CoS_2$ by the introduction of CoS_2 from UV–Vis result, the low AQYs at 450 and 520 nm further verified the cocatalyst function of CoS_2. It was known from Table S1 that, compared with most of the g-C_3N_4 loaded with noble-metal-free sulfide cocatalysts in recent years, CN-$3CoS_2$ showed the better photocatalytic ability for H_2 evolution under visible-light irradiation.

In order to explore the enhancement mechanism of photocatalytic ability by the synchronous construction of CoS_2 in-situ loading and S doping, PL, HER and photoelectrochemical characterizations were carried out. As observed from Fig. 3b, compared with CN, CN-HTS had a weaker characteristic peak, meaning that the recombination of photo-generated carriers in g-C_3N_4 was inhibited by S doping [63]. Moreover, CN-$3CoS_2$ showed weaker PL characteristic peak than CN-HTS, indicating that CoS_2 in-situ loading together with S doping could effectively enhance the separation of photo-generated carriers and then hamper their internal recombination. It was attributed to the fact that CoS_2 acting as the H_2-evolution cocatalyst induced and trapped photo-generated electrons which could effectively transfer from S-doped g-

C_3N_4 to CoS_2 by the Co-S bonding, then promoting the separation of photo-generated carriers. HER properties of CN-E, CN-HTS-E and CN-CoS_2-E are shown in Fig. 3c. Better HER performance of CN-HTS-E than CN-E proved that S doping could improve HER ability of g-C_3N_4. Meanwhile, CN-CoS_2-E had the best HER performance among them, and showed a positive-shift overpotential (0.05 V at 1 mA cm^{-2}) compared with CN-HTS-E. The positive-shift overpotential should be due to the introduction of CoS_2, further proving the effective cocatalyst function of CoS_2 corresponding to the photocatalytic result. To further investigate separation and transfer of photo-generated carriers in g-C_3N_4 by the synchronous construction of CoS_2 in-situ loading and S doping, photoelectrochemical properties of CN-PA and CN-CoS_2-PA were analyzed and seen in Fig. 3d and 3e. From transient photocurrent densities in Fig. 3d, CN-CoS_2-PA showed higher photocurrent than CN-PA, which further proved that the synchronous construction of CoS_2 in-situ loading and S doping promoted the photoelectrochemical ability of g-C_3N_4. Moreover, EIS spectra in Fig. 3e exhibited that CN-CoS_2-PA had a smaller arc radius than CN-PA. It meant that the interfacial charge transfer impedance in CN-CoS_2-PA was decreased by the synchronous construction of CoS_2 in-situ loading and S doping, which was helpful to enhance separation and transfer of photo-generated carriers [64]. It further proved that the synchronous construction of CoS_2 in-situ loading and S doping could enhance effective separation and transfer of photo-generated carriers in g-C_3N_4.

Therefore, CoS_2 in-situ loading and S doping for g-C_3N_4 were synchronously constructed, which effectively promoted the noble-metal-free visible-light-driven photocatalytic activity for H_2 evolution. As observed from Fig. 4, electrons and holes are generated by S-doped g-C_3N_4 under visible-light irradiation. Photo-generated electrons then migrate to CoS_2 by the constructed Co-S bonding between CoS_2 and S-doped g-C_3N_4, and react with water for H_2 evolution, while photo-generated holes stay on S-doped g-C_3N_4 and have oxidation reactions with TEOA on the surface of S-doped g-C_3N_4. The enhanced photocatalytic performance of g-C_3N_4 for H_2 evolution should be mainly attributed to several factors as follows. Firstly, S doping could enhance the visible-light absorption of g-C_3N_4, which is beneficial to excite more generation of photo-generated carriers. Secondly, CoS_2 as the effective H_2-evolution cocatalyst induces and captures photo-generated electrons, then promoting separation of photo-generated carriers synergistically with S doping, and the in-situ growth of CoS_2 nanosheets on the surface of g-C_3N_4 nanosheets promotes more contact between CoS_2 and g-C_3N_4. It is the most important that the synchronous construction of CoS_2 in-situ loading and S doping could enhance effective combination between CoS_2 and S-doped g-C_3N_4, and promote the formation of Co-S bonding between CoS_2 and S-doped g-C_3N_4, strengthening the directed transfer of photo-generated electrons from S-doped g-C_3N_4 to CoS_2 for photocatalytic H_2-evolution reaction.

4. Conclusion

In summary, CoS_2 in-situ loading and S doping on g-C_3N_4 were synchronously constructed to obtain favorable noble-metal-free photocatalytic activity for H_2 evolution under visible-light irradiation (11.55 μmol h^{-1}), which was around 578 times that of pure g-C_3N_4, and AQY at 420 nm was up to 1.08%. S doping improved the visible-light absorption ability of g-C_3N_4, promoting the generation of photo-generated carriers. Recombination of photo-generated carriers were effectively inhibited by the synchronous construction of CoS_2 in-situ loading and S doping due to S doping-based electronic structure change of g-C_3N_4, the cocatalysis function of CoS_2, the in-situ growth of CoS_2 nanosheets on the surface of g-C_3N_4 nanosheets, and the close contact (Co-S bonding) between S-doped g-C_3N_4 and CoS_2 for strengthening the directed transfer of photo-generated electrons from S-doped g-C_3N_4 to CoS_2. This work shows the guiding significance to design and develop the high-efficiency g-C_3N_4-based photocatalysts for noble-metal-free photocatalytic H_2 evolution.

Declaration of competing interest

The authors declare that they have no known competing financial interests or personal relationships that could have appeared to influence the work reported in this paper.

Acknowledgment

We thank the financial support from the Basic Science Center Program for Ordered Energy Conversion of the National Natural Science Foundation of China (No. 51888103), the National Key Research and Development Project (No. 2018YFB1502000), the National Natural Science Foundation of China (Nos. 51961165103, 51302212 and 51906197), the Natural Science Foundation of Shaanxi Province (2020JQ-040) and the Fundamental Research Funds for the Central Universities. We thank the Instrument Analysis Center of Xi'an Jiaotong University for their assistance with TEM analysis.

Appendix A. Supplementary data

Supplementary data to this article can be found online at https://doi.org/10.1016/j.cej.2020.126135.

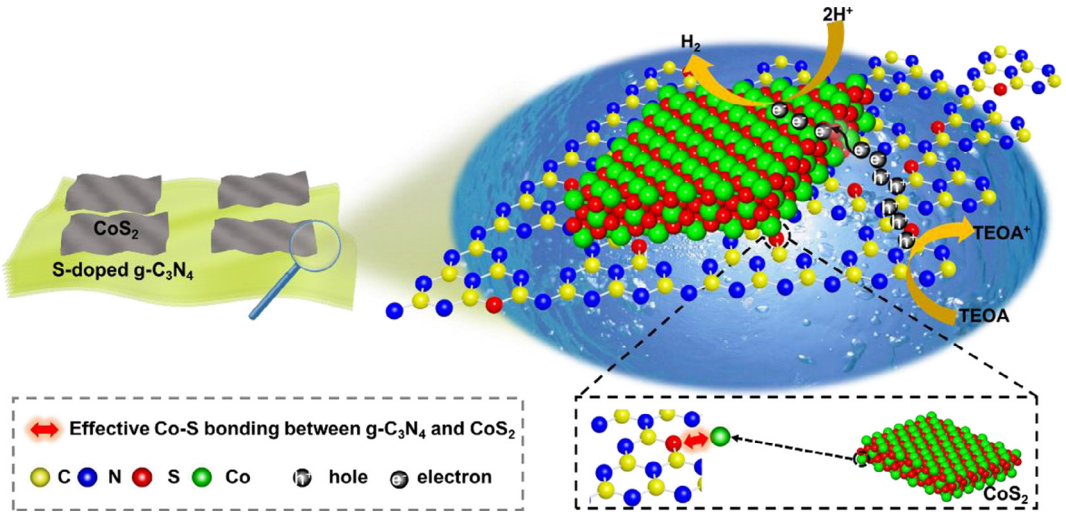

Fig. 4. Illustration of the mechanism about enhanced photocatalytic ability for CoS_2/S-doped g-C_3N_4.

References

[1] A. Kudo, Y. Miseki, Heterogeneous photocatalyst materials for water splitting, Chem. Soc. Rev. 38 (2009) 253–278.
[2] X. Chen, S. Shen, L. Guo, S.S. Mao, Semiconductor-based photocatalytic hydrogen generation, Chem. Rev. 110 (2010) 6503–6570.
[3] A. Fujishima, K. Honda, Electrochemical photolysis of water at a semiconductor electrode, Nature 238 (1972) 37.
[4] S. Linic, P. Christopher, D.B. Ingram, Plasmonic-metal nanostructures for efficient conversion of solar to chemical energy, Nat. Mater. 10 (2011) 911.
[5] T. Takata, K. Domen, Particulate photocatalysts for water splitting: recent advances and future prospects, ACS Energy Lett. 4 (2019) 542–549.
[6] X. Chen, L. Liu, Y.Y. Peter, S.S. Mao, Increasing solar absorption for photocatalysis with black hydrogenated titanium dioxide nanocrystals, Science 331 (2011) 746–750.
[7] Q. Xiang, J. Yu, M. Jaroniec, Synergetic effect of MoS_2 and graphene as cocatalysts for enhanced photocatalytic H_2 production activity of TiO_2 nanoparticles, J. Am. Chem. Soc. 134 (2012) 6575–6578.
[8] S. Ouyang, H. Tong, N. Umezawa, J. Cao, P. Li, Y. Bi, Y. Zhang, J. Ye, Surface-alkalinization-induced enhancement of photocatalytic H_2 evolution over $SrTiO_3$-based photocatalysts, J. Am. Chem. Soc. 134 (2012) 1974–1977.
[9] J. Shi, J. Ye, L. Ma, S. Ouyang, D. Jing, L. Guo, Site-selected doping of upconversion luminescent Er^{3+} into $SrTiO_3$ for visible-light-driven photocatalytic H_2 or O_2 evolution, Chem. – Eur. J. 18 (2012) 7543–7551.
[10] K. Chang, M. Li, T. Wang, S. Ouyang, P. Li, L. Liu, J. Ye, Drastic layer-number-dependent activity enhancement in photocatalytic H_2 evolution over $nMoS_2/CdS$ ($n \geq 1$) under visible light, Adv. Energy Mater. 5 (2015) 1402279.
[11] M. Liu, L. Wang, G.M. Lu, X. Yao, L. Guo, Twins in $Cd_{1-x}Zn_xS$ solid solution: highly efficient photocatalyst for hydrogen generation from water, Energy Environ. Sci. 4 (2011) 1372–1378.
[12] Y. Zhang, S. Zong, C. Cheng, J. Shi, P. Guo, X. Guan, B. Luo, S. Shen, L. Guo, Rapid high-temperature treatment on graphitic carbon nitride for excellent photocatalytic H_2-evolution performance, Appl. Catal. B Environ. 233 (2018) 80–87.
[13] C. Li, Y. Du, D. Wang, S. Yin, W. Tu, Z. Chen, M. Kraft, G. Chen, R. Xu, Unique P-Co-N surface bonding states constructed on g-C_3N_4 nanosheets for drastically enhanced photocatalytic activity of H_2 evolution, Adv. Funct. Mater. 27 (2017) 1604328.
[14] H. Che, G. Che, P. Zhou, C. Liu, H. Dong, C. Li, N. Song, C. Li, Nitrogen doped carbon ribbons modified g-C_3N_4 for markedly enhanced photocatalytic H_2-production in visible to near-infrared region, Chem. Eng. J. 382 (2020) 122870.
[15] X. Wu, D. Gao, H. Yu, J.Yu. Wu, High-yield lactic acid-mediated route for a g-C_3N_4 nanosheet photocatalyst with enhanced H_2-evolution performance, Nanoscale 11 (2019) 9608–9616.
[16] K. Maeda, T. Takata, M. Hara, N. Saito, Y. Inoue, H. Kobayashi, K. Domen, GaN:ZnO solid solution as a photocatalyst for visible-light-driven overall water splitting, J. Am. Chem. Soc. 127 (2005) 8286–8287.
[17] F. Dionigi, P.C. Vesborg, T. Pedersen, O. Hansen, S. Dahl, A. Xiong, K. Maeda, K. Domen, Gas phase photocatalytic water splitting with $Rh_{2-y}Cr_yO_3$/GaN:ZnO in μ-reactors, Energy Environ. Sci. 4 (2011) 2937–2942.
[18] R. Godin, T. Hisatomi, K. Domen, J.R. Durrant, Understanding the visible-light photocatalytic activity of GaN:ZnO solid solution: the role of $Rh_{2-y}Cr_yO_3$ cocatalyst and charge carrier lifetimes over tens of seconds, Chem. Sci. 9 (2018) 7546–7555.
[19] X. Wang, K. Maeda, A. Thomas, K. Takanabe, G. Xin, J.M. Carlsson, K. Domen, M. Antonietti, A metal-free polymeric photocatalyst for hydrogen production from water under visible light, Nat. Mater. 8 (2009) 76.
[20] G. Liu, T. Wang, H. Zhang, X. Meng, D. Hao, K. Chang, P. Li, T. Kako, J. Ye, Nature-inspired environmental "phosphorylation" boosts photocatalytic H_2 production over carbon nitride nanosheets under visible-light irradiation, Angew. Chem. Int. Ed. 54 (2015) 13561–13565.
[21] Y. Zou, J. Shi, L. Sun, D. Ma, S. Mao, Y. Lv, Y. Cheng, Energy-band-controlled $Zn_xCd_{1-x}In_2S_4$ solid solution coupled with g-C_3N_4 nanosheets as 2D/2D heterostructure toward efficient photocatalytic H_2 evolution, Chem. Eng. J. 378 (2019) 122192.
[22] W. Iqbal, B. Yang, X. Zhao, M. Rauf, M. Waqas, Y. Gong, J. Zhang, Y. Mao, Controllable synthesis of graphitic carbon nitride nanomaterials for solar energy conversion and environmental remediation: the road travelled and the way forward, Catal. Sci. Technol. 8 (2018) 4576–4599.
[23] J. Ran, J. Zhang, J. Yu, M. Jaroniec, S.Z. Qiao, Earth-abundant cocatalysts for semiconductor-based photocatalytic water splitting, Chem. Soc. Rev. 43 (2014) 7787–7812.
[24] X. Wu, H. Ma, W. Zhong, J. Fan, H. Yu, Porous crystalline g-C_3N_4: bifunctional $NaHCO_3$ template-mediated synthesis and improved photocatalytic H_2-evolution rate, Appl. Catal. B Environ. 271 (2020) 118899.
[25] N. Mahmood, Y. Yao, J.W. Zhang, L. Pan, X. Zhang, J.J. Zou, Electrocatalysts for hydrogen evolution in alkaline electrolytes: mechanisms, challenges, and prospective solutions, Adv. Sci. 5 (2018) 1700464.
[26] X. Zou, Y. Zhang, Noble metal-free hydrogen evolution catalysts for water splitting, Chem. Soc. Rev. 44 (2015) 5148–5180.
[27] H. Li, P. Deng, Y. Hou, Cobalt disulfide/graphitic carbon nitride as an efficient photocatalyst for hydrogen evolution reaction under visible light irradiation, Mater. Lett. 229 (2018) 217–220.
[28] H. Zhao, S. Sun, P. Jiang, Z.J. Xu, Graphitic C_3N_4 modified by Ni_2P cocatalyst: an efficient, robust and low cost photocatalyst for visible-light-driven h_2 evolution from water, Chem. Eng. J. 315 (2017) 296–303.
[29] A. Indra, A. Acharjya, P.W. Menezes, C. Merschjann, D. Hollmann, M. Schwarze, M. Aktas, A. Friedrich, S. Lochbrunner, A. Thomas, Boosting visible-light-driven photocatalytic hydrogen evolution with an integrated nickel phosphide-carbon nitride system, Angew. Chem. Int. Ed. 56 (2017) 1653–1657.
[30] H. Zhao, H. Zhang, G. Cui, Y. Dong, G. Wang, P. Jiang, X. Wu, N. Zhao, A photochemical synthesis route to typical transition metal sulfides as highly efficient cocatalyst for hydrogen evolution: from the case of NiS/g-C_3N_4, Appl. Catal. B Environ. 225 (2018) 284–290.
[31] H. Zhao, P. Jiang, W. Cai, Graphitic C_3N_4 decorated with CoP co-catalyst: enhanced and stable photocatalytic H_2 evolution activity from water under visible-light irradiation, Chem. - Eur. J. 12 (2017) 361–365.
[32] R. Shen, J. Xie, H. Zhang, A. Zhang, X. Chen, X. Li, Enhanced solar fuel H_2 generation over g-C_3N_4 nanosheet photocatalysts by the synergetic effect of noble metal-free Co_2P cocatalyst and the environmental phosphorylation strategy, ACS Sustainable Chem. Eng. 6 (2018) 816–826.
[33] H. Zhao, J. Wang, Y. Dong, P. Jiang, Noble-metal-free iron phosphide cocatalyst loaded graphitic carbon nitride as an efficient and robust photocatalyst for hydrogen evolution under visible light irradiation, ACS Sustainable Chem. Eng. 5 (2017) 8053–8060.
[34] R. Shen, J. Xie, X. Lu, X. Chen, X. Li, Bifunctional Cu_3P decorated g-C_3N_4 nanosheets as a highly active and robust visible-light photocatalyst for H_2 production, ACS Sustainable Chem. Eng. 6 (2018) 4026–4036.
[35] G. Zhang, G. Li, X. Wang, Surface modification of carbon nitride polymers by core-shell nickel/nickel oxide cocatalysts for hydrogen evolution photocatalysis, ChemCatChem 27 (2015) 2864–2870.
[36] H. Yu, P. Xiao, P. Wang, J. Yu, Amorphous molybdenum sulfide as highly efficient electron-cocatalyst for enhanced photocatalytic H_2 evolution, Appl. Catal. B Environ. 193 (2016) 217–225.
[37] C. Xue, H. Li, H. An, B. Yang, J. Wei, G. Yang, NiS_x quantum dots accelerate electron transfer in $Cd_{0.8}Zn_{0.2}S$ photocatalytic system via an rGO nanosheet "bridge" toward visible-light-driven hydrogen evolution, ACS Catal. 8 (2018) 1532–1545.
[38] J. Fu, C. Bie, B. Cheng, C. Jiang, J. Yu, Hollow CoS_x polyhedrons act as high-efficiency cocatalyst for enhancing the photocatalytic hydrogen generation of g-C_3N_4, ACS Sustainable Chem. Eng. 6 (2018) 2767–2779.
[39] Z.F. Huang, J. Song, K. Li, M. Tahir, Y.T. Wang, L. Pan, L. Wang, X. Zhang, J.J. Zou, Hollow cobalt-based bimetallic sulfide polyhedra for efficient all-pH-value electrochemical and photocatalytic hydrogen evolution, J. Am. Chem. Soc. 138 (2016) 1359–1365.
[40] Y.S. Zhu, Y. Xu, Y.D. Hou, Z.X. Ding, X.C. Wang, Cobalt sulfide modified graphitic carbon nitride semiconductor for solar hydrogen production, Int. J. Hydrogen Energ 39 (2014) 11873–11879.
[41] X. Liu, J. He, S. Zhao, Y. Liu, Z. Zhao, J. Luo, G. Hu, X. Sun, Y. Ding, Self-powered H_2 production with bifunctional hydrazine as sole consumable, Nat. Commun. 9 (2018) 4365.
[42] K. Afroz, M. Moniruddin, N. Bakranov, S. Kudaibergenov, N. Nuraje, A heterojunction strategy to improve the visible light sensitive water splitting performance of photocatalytic materials, J. Mater. Chem. A 6 (2018) 21696–21718.
[43] G. Liu, P. Niu, C. Sun, S.C. Smith, Z. Chen, G.Q. Lu, H.M. Cheng, Unique electronic structure induced high photoreactivity of sulfur-doped graphitic C_3N_4, J. Am. Chem. Soc. 132 (2010) 11642–11648.
[44] H. Qin, W. Lv, J. Bai, Y. Zhou, Y. Wen, Q. He, J. Tang, L. Wang, Q. Zhou, Sulfur-doped porous graphitic carbon nitride heterojunction hybrids for enhanced photocatalytic H_2 evolution, J. Mater. Sci. 54 (2018) 4811–4820.
[45] H. Wang, Y. Bian, J. Hu, L. Dai, Highly crystalline sulfur-doped carbon nitride as photocatalyst for efficient visible-light hydrogen generation, Appl. Catal. B Environ. 238 (2018) 592–598.
[46] M. Wu, Y. Gong, T. Nie, J. Zhang, R. Wang, H. Wang, B. He, Template-free synthesis of nanocage-like g-C_3N_4 with high surface area and nitrogen defects for enhanced photocatalytic H_2 activity, J. Mater. Chem. A 7 (2019) 5324–5332.
[47] G. Ge, X. Guo, C. Song, Z. Zhao, Reconstructing supramolecular aggregates to nitrogen-deficient g-C_3N_4 bunchy tubes with enhanced photocatalysis for H_2 production, ACS Appl. Mater. Interfaces 10 (2018) 18746–18753.
[48] L. Jin, B. Liu, Y. Wu, S. Thanneeru, J. He, Synthesis of mesoporous CoS_2 and $Ni_xCo_{1-x}S_2$ with superior supercapacitive performance using a facile solid-phase sulfurization, ACS Appl. Mater. Interfaces 9 (2017) 36837–36848.
[49] H. Yu, R. Shi, Y. Zhao, T. Bian, Y. Zhao, C. Zhou, G.I.N. Waterhouse, L.Z. Wu, C.H. Tung, T. Zhang, Alkali-assisted synthesis of nitrogen deficient graphitic carbon nitride with tunable band structures for efficient visible-light-driven hydrogen evolution, Adv. Mater. 29 (2017) 1605148.
[50] W. Che, W. Cheng, T. Yao, F. Tang, W. Liu, H. Su, Y. Huang, Q. Liu, J. Liu, F. Hu, Z. Pan, Z. Sun, S. Wei, Fast photoelectron transfer in (C_{ring})-C_3N_4 plane heterostructural nanosheets for overall water splitting, J. Am. Chem. Soc. 139 (2017) 3021–3026.
[51] T. Zhang, J. Wu, Y. Xu, X. Wang, J. Ni, Y. Li, J.W. Niemantsverdriet, Cobalt and cobalt carbide on alumina/NiAl(110) as model catalysts, Catal. Sci. Technol. 7 (2017) 5893–5899.
[52] J.Y. Zhang, W. Xiao, P.X. Xi, S.B. Xi, Y.H. Du, D.Q. Gao, J. Ding, Activating and optimizing activity of CoS_2 for hydrogen evolution reaction through the synergic effect of N dopants and S vacancies, ACS Energy Lett. 2 (2017) 1022–1028.
[53] F. Xue, M. Liu, C. Cheng, J. Deng, J. Shi, Localized NiS_2 Quantum dots on g-C_3N_4 nanosheets for efficient photocatalytic hydrogen production from water, ChemCatChem 10 (2018) 5441–5448.
[54] C. Sun, H. Zhang, H. Liu, X. Zheng, W. Zou, L. Dong, L. Qi, Enhanced activity of visible-light photocatalytic H_2 evolution of sulfur-doped g-C_3N_4 photocatalyst via nanoparticle metal Ni as cocatalyst, Appl. Catal. B Environ. 235 (2018) 66–74.
[55] M.-H. Vu, M. Sakar, C.-C. Nguyen, T.-O. Do, Chemically bonded Ni cocatalyst onto the S doped g-C_3N_4 nanosheets and their synergistic enhancement in H_2 production under sunlight irradiation, ACS Sustainable Chem. Eng. 6 (2018) 4194–4203.

[56] L. Bi, X. Gao, L. Zhang, D. Wang, X. Zou, T. Xie, Enhanced photocatalytic hydrogen evolution of NiCoP/g-C_3N_4 with improved separation efficiency and charge transfer efficiency, ChemSusChem 11 (2018) 276–284.
[57] H. Chen, D. Jiang, Z. Sun, R.M. Irfan, L. Zhang, P. Du, Cobalt nitride as an efficient cocatalyst on CdS nanorods for enhanced photocatalytic hydrogen production in water, Catal. Sci. Technol. 7 (2017) 1515–1522.
[58] G. Zhang, S. Zang, X. Wang, Layered $Co(OH)_2$ deposited polymeric carbon nitrides for photocatalytic water oxidation, ACS Catal. 5 (2015) 941–947.
[59] Y. Zhang, J. Shi, C. Cheng, S. Zong, J. Geng, X. Guan, L. Guo, Hydrothermal growth of $Co_3(OH)_2(HPO_4)_2$ nano-needles on $LaTiO_2N$ for enhanced water oxidation under visible-light irradiation, Appl. Catal. B Environ. 232 (2018) 268–274.
[60] S. Stolbov, S. Zuluaga, Sulfur doping effects on the electronic and geometric structures of graphitic carbon nitride photocatalyst: insights from first principles, J. Phys.: Condens. Matter 25 (2013) 085507.
[61] J. Hong, X. Xia, Y. Wang, R. Xu, Mesoporous carbon nitride with in situ sulfur doping for enhanced photocatalytic hydrogen evolution from water under visible light, J. Mater. Chem. 22 (2012) 15006–15012.
[62] S. Cao, J. Low, J. Yu, M. Jaroniec, Polymeric photocatalysts based on graphitic carbon nitride, Adv. Mater. 27 (2015) 2150–2176.
[63] J. Xie, S.A. Shevlin, Q. Ruan, S.J. Moniz, Y. Liu, X. Liu, Y. Li, C.C. Lau, Z.X. Guo, J. Tang, Efficient visible light-driven water oxidation and proton reduction by an ordered covalent triazine-based framework, Energy Environ. Sci. 11 (2018) 1617–1624.
[64] C. Cheng, S. Zong, J. Shi, F. Xue, Y. Zhang, X. Guan, B. Zheng, J. Deng, L. Guo, Facile preparation of nanosized MoP as cocatalyst coupled with g-C_3N_4 by surface bonding state for enhanced photocatalytic hydrogen production, Appl. Catal. B Environ. 265 (2020) 118620.